PHYSICAL REVIEW B **87**, 201401(R) (2013)

Observation of intense second harmonic generation from MoS_2 atomic crystals

Leandro M. Malard,[1] Thonimar V. Alencar,[1] Ana Paula M. Barboza,[1] Kin Fai Mak,[2] and Ana M. de Paula[1,*]

[1]*Department of Physics, Federal University of Minas Gerais, 30123-970 Belo Horizonte-MG, Brazil*

[2]*Department of Physics, Columbia University, New York, New York 10027, USA*

(Received 4 January 2013; revised manuscript received 26 March 2013; published 13 May 2013)

The nonlinear optical properties of few-layer MoS_2 two-dimensional crystals are studied using femtosecond laser pulses. We observed highly efficient second-harmonic generation from the odd-layer crystals, which shows a polarization intensity dependence that directly reveals the underlying symmetry and orientation of the crystal. Additionally, the measured second-order susceptibility spectra provide information about the electronic structure of the material. Our results open up opportunities for studying the nonlinear optical properties in these two-dimensional crystals.

DOI: 10.1103/PhysRevB.87.201401 PACS number(s): 42.65.Ky, 42.70.Mp, 78.67.−n, 81.05.Hd

The family of two-dimensional (2D) transition-metal dichalcogenide semiconductors MX_2 (M stands for Mo or W; and X stands for S, Se, or Te) has attracted much recent attention. These materials are direct band-gap semiconductors that possess properties very different from graphene.[1–11] For instance, single layer MoS_2 shows efficient light emission,[5,6] optical control of valley polarization,[7–9] enhanced many-body interactions,[12] and transistors with high on-off ratios.[13,14] These properties are not only important for applications in electronics and optoelectronics with 2D crystals but the associated valley-dependent physics and topological transport phenomena[15] are also of fundamental interest.

The lack of an inversion center in the crystalline structure of the material (so that energy gaps at the K and K′ valleys with finite but opposite Berry curvatures are introduced) is the underlying reason for developing interesting properties. Actually, the inversion asymmetry of the material not only affects its electronic and linear optical properties but also gives rise to a finite second-order optical nonlinearity ($\chi^{(2)} \neq 0$).[16,17] The finite $\chi^{(2)}$ provides opportunities for new applications in optoelectronics devices (e.g., coherent control of valley-polarized currents) that are not possible with graphene.

Here we report the observation of intense second-harmonic generation (SHG) from odd-layered MoS_2 thin films. In contrast, very low SHG is observed for samples with even-layer numbers due to the restoration of inversion symmetry. Moreover, the threefold rotation symmetry of the crystal produces a characteristic sixfold polarization dependence pattern for the SHG intensity, from which we have developed an optical method for imaging the underlying crystalline structure and domain orientations with submicron resolution. We have also measured the $\chi^{(2)}$ spectra by varying the incident pump photon energy. Comparison to absorption measurements shows that the observed efficient SHG comes from resonant enhancement due to the optical transitions in the near UV range.

The mono- and few-layer MoS_2 samples were obtained by mechanical exfoliation of natural bulk hexagonal MoS_2, which is deposit in Si covered with 300-nm SiO_2 substrates[1] or on transparent amorphous quartz (SPI Supplies, Inc.). We have characterized the MoS_2 layer number with a combination of optical microscopy, atomic force microscopy (AFM),[18] Raman spectroscopy,[18] and photoluminescence imaging.[5] For the second-harmonic imaging we used a 140-fs Ti-Sapphire oscillator (Coherent Chameleon) with 80-MHz repetition and tunable wavelength from 680 to 1080 nm, which is directed to a confocal scanning laser microscope (Olympus FV300) modified for two photon excitation. The laser is focused on the sample at normal incidence by a 60× objective (NA 0.75). The back reflected signal is then directed to a dichroic mirror and a thin bandpass centered at the SH wavelength to completely remove the laser scattered light, and the SH signal is detected by a photomultiplier tube.

Figure 1(a) shows the optical images of mono- and few-layer MoS_2 samples, where the colors indicate the number of layers.[19] Figure 1(b) shows the sample characterization by AFM at the dashed triangle area marked in Fig. 1(a). By measuring the height of MoS_2 relative to the substrate[18] we found regions of MoS_2 monolayer (1L), bilayer (2L), and trilayer (3L), respectively, as indicated by the labels in Fig. 1(b) (see Supplemental Materials for details[20]). Figure 1(c) presents the sample second-harmonic image, the same area as in Fig. 1(a), showing well-defined regions where the second-harmonic intensity varies. To unambiguously show that the strong optical emission in Fig. 1(c) is due to the optical second-harmonic generation, we measured its intensity dependence on pump-laser power, as shown in Fig. 1(d). Since SHG is a second-order nonlinear optical process, the SHG intensity scales quadratically with the fundamental pump intensity.[16,17] This is in agreement with our results shown in Fig. 1(d), where the log scale plot shows a linear dependence with a slope equal to 2.00 ± 0.02.

To visualize the spatial variation of the second-harmonic intensity as a function of the MoS_2 ultra-thin-film position we plot the SHG intensity profile in log scale, Fig. 1(e), at the marked yellow line in Fig. 1(c). It is intriguing to observe that a stronger signal is present for the monolayer MoS_2 when compared to the trilayer MoS_2, for the pump wavelength at 800 nm, considering that less material is present in the former case. Also, the bilayer MoS_2 shows very low second-harmonic generation, almost two orders of magnitude lower than the monolayer. The small observed signal may come from the boundary between the layers.[21,22] The $\chi^{(2)}$ tensor holds the information of the crystallographic properties of the crystal[16,17] and for SHG without phase matching determines the SHG intensity. This is true for the present case, where the

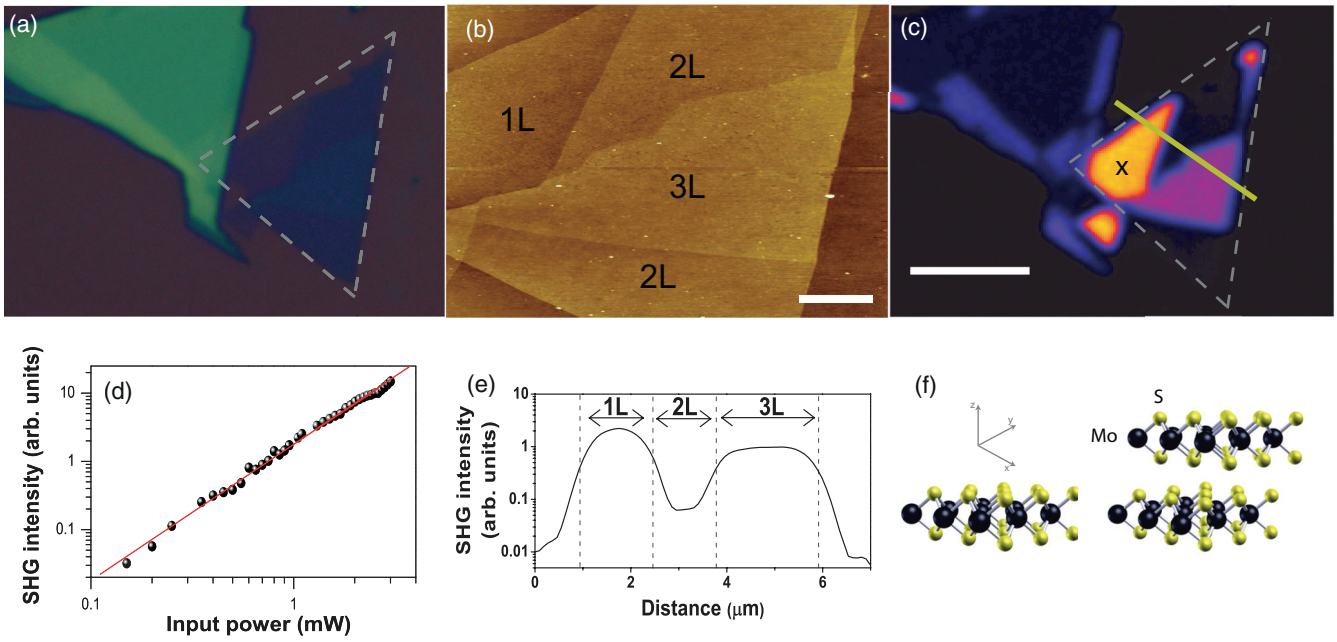

FIG. 1. (Color online) (a) Optical microscope image of the MoS_2 thin film. (b) AFM image of the same MoS_2 thin film made within the dashed triangle shown in part a, scale bar 1 μm. By measuring the height relative to the substrate, the number of MoS_2 layers are determined as 1L for monolayer, 2L for bilayer, and 3L for trilayer MoS_2. (c) Second-harmonic image collected from the same MoS_2 thin film, pump-laser wavelength at 800 nm, 1.55 eV. Brighter colors mean stronger SHG intensity, and the scale bar is 5 μm. (d) Log vs log plot of the power dependence of SHG from the X marked position in part c. The circles are the measured data, and the red line is a linear fit of the data with an extracted slope of 2.00 ± 0.02. (e) Intensity profile of the SHG image from left to right at the yellow line shown in part c. (f) Atomic structure of monolayer (left) and bilayer (right) MoS_2.

sample thickness is much smaller than the light wavelength. Hence, in order to understand this spatial intensity variation, we should determine each element of the tensor to directly probe the crystal structure of two-dimensional MoS_2.

The bulk MoS_2 crystal has a trigonal prismatic structure with Bernal stacking;[23] thus, it belongs to the $P6_3/mmc$ nonsymmorphic space group,[23,24] with an inversion symmetry operation in the middle of the two MoS_2 monolayers. The monolayer and bilayer MoS_2 structures are shown in Fig. 1(f). As the layer number decreases down to one monolayer of MoS_2, it is convenient to make the point-group representation of the unit cell, which is composed of three atoms (one Mo and two S). Therefore we assign the symmetry of the monolayer as D_{3h}, since the inversion symmetry present in bulk MoS_2 is lost. However, in bilayer MoS_2 the inversion symmetry operation is again present; nonetheless, due to the lack of translation symmetry along the z axis, the point group is D_{3d}. In general, an even number of layers belongs to the D_{3d} point group and an odd number of layers belongs to the D_{3h} point group (similar to few-layer graphene point groups[25]). This simple approach can explain qualitatively the absence of second-harmonic generation in bilayer MoS_2: due to the presence of inversion symmetry the $\chi^{(2)}$ tensor is equal to zero; thus, no second harmonic is generated for bilayer MoS_2 within the dipole approximation.[16,17] Generally speaking, there is no second-harmonic generation for an even MoS_2 layer number, but it can be generated in an odd number of MoS_2 layers. We should note that we also studied monolayer graphene exfoliated on transparent amorphous quartz and observed no significant SHG signal, as is expected from the symmetry of the crystal.

Due to the sensitivity of the SHG to the crystal symmetry, polarization-resolved SHG measurements provide important crystallographic information of MoS_2 atomic layers. To measure the polarization dependence of the SHG, we have placed the sample on top of a precision rotation stage, which is placed under the microscope objective. The laser (at 800 nm) is focused on the sample at normal incidence and with a fixed linear polarization that is in the plane of the sample. The sample is initially with the crystallographic axis at an arbitrary angle to the incident polarization. We have measured one SH image for each sample angle, at 5-deg steps, for the SH polarization parallel to that of the incident laser (a polarization analyzer is placed before the detector to select the SH polarization).

Figure 2(a) shows the experimental results of the SHG polarization dependence for the monolayer of MoS_2 in Fig. 1(c), where the second-harmonic intensity is plotted as a function of the sample rotation angle. A clear sixfold pattern can be observed in Fig. 2(a). In Fig. 2(b) is a sketch of a top view showing the angle of the MoS_2 crystallographic orientation to the incident laser polarization direction ($\hat{e}_\omega$). Figure 2(c) shows the SH images for the monolayer and trilayer MoS_2 samples together with the crystallographic orientation of the crystal lattice obtained from the polarization data in Fig. 2(a). To obtain the crystallographic orientation, we first describe the electric field of the generated second-harmonic light [$\mathbf{E}(2\omega)$] along a given direction ($\hat{e}_{2\omega}$) in terms of the $\chi^{(2)}$

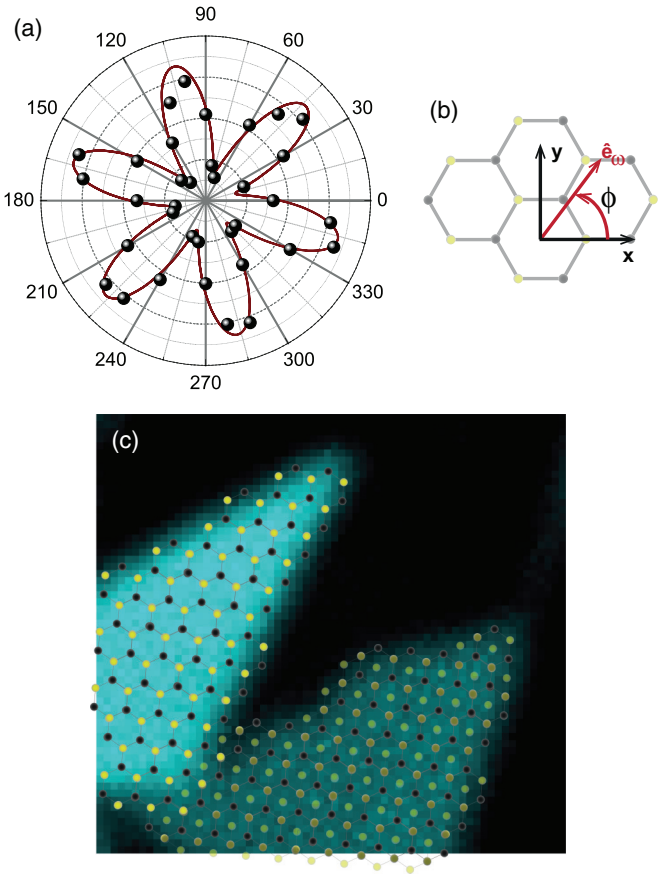

FIG. 2. (Color online) (a) Polar plot of the second-harmonic intensity from monolayer MoS_2 as a function of the sample angle. (b) Top view of the MoS_2 crystallographic orientation with respect to the incident laser polarization ($\hat{e}_\omega$). (c) SH image of the same sample as in Fig. 1(c) showing the crystallographic direction of the monolayer and trilayer MoS_2 sample determined by our polarization measurements.

tensor and input light polarization vector ($\hat{e}_\omega$) as[16,17]

$$\mathbf{E}(2\omega)\cdot\hat{e}_{2\omega} = C\hat{e}_{2\omega}\cdot\chi^{(2)}:\hat{e}_\omega\hat{e}_\omega, \qquad (1)$$

where ω is the laser frequency, 2ω is the SH frequency, and C is a proportionality constant which contains local-field factors determined by the local dielectric environment. Equation (1) fully describes the polarization dependence of the SHG, and its specific form will depend on the $\chi^{(2)}$ tensor. For the odd layer with D_{3h} point-group symmetry, the second-order susceptibility tensor has a single nonzero element:[16,17] $\chi^{(2)}_{MoS_2} \equiv \chi^{(2)}_{xxx} = -\chi^{(2)}_{xyy} = -\chi^{(2)}_{yyx} = -\chi^{(2)}_{yxy}$, where x corresponds to the armchair direction, since it has a mirror plane symmetry,[16,17] and y is the zigzag direction [see Fig. 2(b)]. Thus, using Eq. (1) we obtain the resulting dependence of the generated second-harmonic electric field as a function of the sample angle for a pump-laser polarization ($\hat{e}_\omega$) parallel to the analyzer ($\hat{e}_{2\omega}$), that can be expressed as[16,17]

$$E(2\omega) = C\chi^{(2)}_{MoS_2}\cos(3\phi+\phi_0), \qquad (2)$$

where ϕ is the angle between the input laser polarization and the x direction and ϕ_0 is the initial crystallographic orientation of the MoS_2 sample. It is worth mentioning that for the analyzer at crossed polarization with the input laser the second-harmonic electric field is proportional to $\sin(3\phi+\phi_0)$; hence, the total SH intensity (without the analyzer) is constant with θ. The intensity of the generated second-harmonic light as a function of the sample angle is obtained from Eq. (2),[16,17] resulting in $I_{2\omega} \propto \cos^2(3\phi+\phi_0)$. Using this intensity dependence of the second harmonic with the sample angle, we have fitted the experimental data as shown in Fig. 2(a). The fitting shown by the red lines agrees with the experimental data within $\phi_0 = 16 \pm 5$ deg, indicating that the armchair (x) of MoS_2 was initially rotated with respect to the input laser polarization. We should note that as our measurement is phase insensitive there is an arbitrariness of 60 deg in the definition of the x axis.

This result shows that from this simple approach one can measure the crystallographic direction of MoS_2 purely by optical means. As an example of the application of this technique, we have shown in Fig. 2(c) the SH image of the monolayer and trilayer MoS_2 samples together with the crystallographic orientation of the crystal lattice determined by the polarization measurement in Fig. 2(a). This method can be used for future applications in materials where it is important to determine the crystallographic directions. Two well-known examples are the 2D heterostructures (i.e., stacks of different 2D crystals) and nanoribbons,[26–28] where the physical properties depend on the relative 2D crystal stacking orientation and the edge atomic structure, respectively.

The SHG can provide also valuable information about the electronic structure of crystals. Hence, we have measured SHG intensity as a function of the incident laser wavelength for the monolayer and trilayer. For these measurements the laser beam was redirected to a home-built microscope with 60× objective, 0.75 NA, giving a spot size of 1.2 μm in diameter at the sample focal plane. The backscattered light is collected and sent to a spectrometer and detected by a charge coupled device (CCD) with a set of filters to remove the pump-laser light. In order to avoid any spectral dependence of the SHG signal coming from our experimental setup, we have used the same laser power, and we have verified that the spot size does not change significantly for the different laser lines used. Also, the spectral dependences of the spectrometer, collection optics, and CCD camera were normalized by using a calibration lamp (Ocean Optics).

Figure 3(a) shows an optical image of the MoS_2 sample on transparent amorphous quartz, where we have characterized the monolayers, bilayers, trilayers, and quadlayers by AFM. Figures 3(b)–3(d) are SH images of such samples taken under different incident photon energies, where it is possible to observe that by decreasing the laser energy the monolayer and the trilayer SH intensities become very similar [Fig. 3(c)], and in Fig. 3(d) the monolayer intensity becomes slightly smaller as compared to the trilayer.

Figure 3(e) shows the SH signal for the monolayer and trilayer samples as a function of the SH energy, where resonance enhancement peaks are clearly observed. To obtain the second-order sheet susceptibility of MoS_2 atomic layers ($\chi^{(2)sheet}_{MoS_2}$) in SI units, we normalized the SHG intensity from MoS_2 (I_{MoS_2}) to that from alpha quartz (I_{quartz}). For samples on transparent amorphous quartz substrates with bulk inversion symmetry, this can be written as[22] (details in Supplemental

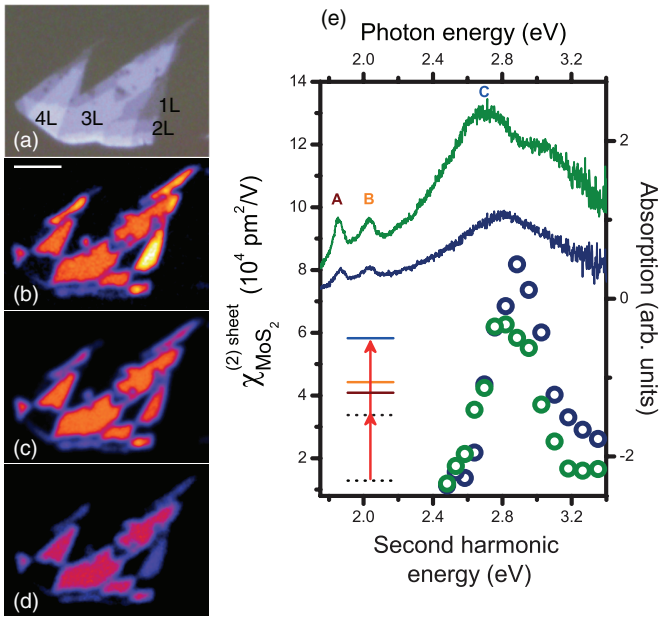

FIG. 3. (Color online) (a) Optical image of the few-layer MoS_2 sample on transparent quartz substrate. The number of layers is indicated as measured by AFM. Parts b–d show the SH image for the same sample with pump-laser wavelength at (b) 860 nm and 1.44 eV, (c) 900 nm and 1.38 eV, and (d) 960 nm and 1.29 eV. (e) Second-order susceptibility, left scale, of a sheet of MoS_2 for monolayer (blue circles) and trilayer (green circles) samples as a function of pump-laser energy, with measured linear absorption (right scale) spectra of monolayer (blue line) and trilayer (green line) with the labeled optical transitions. Inset: Diagram of the second-harmonic enhancement in monolayer MoS_2 where the two-photon energy is in resonance with the C absorption peak.

Materials[20])

$$\frac{\chi^{(2)\mathrm{sheet}}_{MoS_2}}{\chi^{(2)\mathrm{bulk}}_{\mathrm{quartz}}} \approx \frac{\pi N^2 f}{4nk_0} \frac{\sqrt{I_{MoS_2}(2\omega)}/I_{MoS_2}(\omega)}{\sqrt{I_{\mathrm{quartz}}(2\omega)}/I_{\mathrm{quartz}}(\omega)}. \quad (3)$$

Here n is the refractive index of quartz (note that we have neglected the slight spectral variation of n and the small difference of n between amorphous and crystalline quartz), f is a numerical constant that depends on the numerical aperture of the objective, $k_0 = 2\pi/\lambda$ is the magnitude of the vacuum fundamental wave vector, and $\chi^{(2)\mathrm{bulk}}_{\mathrm{quartz}}$ is the bulk susceptibility of alpha quartz. To obtain this formula, we have made use of the expression for reflected SHG intensity from the alpha-quartz surface.[29] We used the $\chi^{(2)\mathrm{bulk}}_{\mathrm{quartz}}$ value as 0.8 ± 0.04 pm/V (see Table 7.1 of Ref. 17).

The $\chi^{(2)\mathrm{sheet}}_{MoS_2}$ for both the monolayer and trilayer samples as a function of the SH energy, that is frequency 2ω, are plotted in Fig. 3(e). Also shown are the normalized absorption spectra of the corresponding samples. We can see that over the specified spectral range there are three peaks known as the A, B, and C excitons. They originate from the direct optical transitions at the K (for the A and B features) and the Γ (for the C feature) point of the Brillouin zone.[5] A significant enhancement of $\chi^{(2)\mathrm{sheet}}_{MoS_2}$ is observed with spectral positions very well matched with the C resonances in the linear absorption spectra (∼2.8 eV for monolayers and ∼2.7 eV for trilayers). It suggests that the resonance enhancement of $\chi^{(2)\mathrm{sheet}}_{MoS_2}$ is originated from the increased density of electronic states at the Γ point [see inset of Fig. 3(e)]. The different resonance position between the monolayers and the trilayers is thus a consequence of the different energy gaps at the Γ point of the Brillouin zone, a modification of the electronic structure from quantum confinement in reduced sample thickness. While the SHG from trilayer $\chi^{(2)\mathrm{sheet}}_{MoS_2}$ is consistently smaller than that of the monolayer for photon energies above the C resonance, it becomes slightly larger than that of the monolayer at lower photon energies. Such an observation demonstrates the perfect cancellation of second-harmonic (SH) dipole moments in an AB-stacked Bernal unit cell.

In summary, our demonstration of strong resonant SHG from monolayer and trilayer MoS_2, although being only a few atoms thick, shows its potential use for nonlinear optical device applications. Also, the SHG dependence on the crystallographic axis and electronic resonance effects opens up an optical way to characterize the crystal structure of many 2D crystals. Furthermore, the ability to distinguish different crystallographic axes can be applied to improve materials properties, such as stacking different 2D materials with atomic registry and edge-defined nanoribbons.

Note added in proof. Recently, somewhat similar results of SHG observation for MoS_2 layers have been published.[30] Also, SHG from similar 2D crystals, WS_2 and WSe_2, have been observed.[31]

This work was supported by Conselho Nacional de Desenvolvimento Científico e Tecnológico (CNPq), Fundação de Amparo à Pesquisa de Minas Gerais (FAPEMIG), and National Institute of Science and Technology on Carbon Nanomaterials, Brazil. The authors thank B. R. A. Neves for assistance with the AFM measurements and T. F. Heinz, A. Jorio, and G. Weber for fruitful discussions.

*ana@fisica.ufmg.br

[1]K. S. Novoselov, D. Jiang, F. Schedin, T. J. Booth, V. V. Khotkevich, S. V. Morozov, and A. K. Geim, PNAS **102**, 10451 (2005).

[2]K. S. Novoselov, Rev. Mod. Phys. **83**, 837 (2011).

[3]J. N. Coleman, M. Lotya, A. O'Neill, S. D. Bergin, P. J. King, U. Khan, K. Young, A. Gaucher, S. De, R. J. Smith, I. V. Shvets, S. K. Arora, G. Stanton, H.-Y. Kim, K. Lee, G. T. Kim, G. S. Duesberg, T. Hallam, J. J. Boland, J. J. Wang, J. F. Donegan, J. C. Grunlan, G. Moriarty, A. Shmeliov, R. J. Nicholls, J. M. Perkins, E. M. Grieveson, K. Theuwissen, D. W. McComb, P. D. Nellist, and V. Nicolosi, Science **331**, 568 (2011).

[4]K. S. Novoselov and A. H. Castro Neto, Phys. Scr. **2012**, 014006 (2012).

[5]K. F. Mak, C. Lee, J. Hone, J. Shan, and T. F. Heinz, Phys. Rev. Lett. **105**, 136805 (2010).

[6] A. Splendiani, L. Sun, Y. Zhang, T. Li, J. Kim, C.-Y. Chim, G. Galli, and F. Wang, Nano Lett. **10**, 1271 (2010).
[7] K. F. Mak, K. He, J. Shan, and T. F. Heinz, Nature Nanotechnology **7**, 494 (2012).
[8] H. Zeng, J. Dai, W. Yao, D. Xiao, and X. Cui, Nature Nanotechnology **7**, 490 (2012).
[9] T. Cao, G. Wang, W. Han, H. Ye, C. Zhu, J. Shi, Q. Niu, P. Tan, E. Wang, B. Liu, and J. Feng, Nat. Commun. **3**, 887 (2012).
[10] S. Tongay, J. Zhou, C. Ataca, K. Lo, T. S. Matthews, J. Li, J. C. Grossman, and J. Wu, Nano Lett. **12**, 5576 (2012).
[11] Q. H. Wang, K. Kalantar-Zadeh, A. Kis, J. N. Coleman, and M. S. Strano, Nature Nanotechnology **7**, 699 (2012).
[12] K. F. Mak, K. He, C. Lee, G. H. Lee, J. Hone, T. F. Heinz, and J. Shan, Nat. Mater. **12**, 207 (2013).
[13] B. Radisavljevic, A. Radenovic, J. Brivio, and V. G. A. Kis, Nature Nanotechnology **6**, 147 (2011).
[14] Z. Yin, H. Li, H. Li, L. Jiang, Y. Shi, Y. Sun, G. Lu, Q. Zhang, X. Chen, and H. Zhang, ACS Nano **6**, 74 (2012).
[15] D. Xiao, G.-B. Liu, W. Feng, X. Xu, and W. Yao, Phys. Rev. Lett. **108**, 196802 (2012).
[16] R. Boyd, *Nonlinear Optics* (Academic, London, 2008).
[17] Y. R. Shen, *The Principles of Nonlinear Optics* (Wiley-Interscience, New York, 2003).
[18] C. Lee, H. Yan, L. E. Brus, T. F. Heinz, J. Hone, and S. Ryu, ACS Nano **4**, 2695 (2010).
[19] M. M. Benameur, B. Radisavljevic, J. S. Héron, S. Sahoo, H. Berger, and A. Kis, Nanotechnology **22**, 125706 (2011).
[20] See Supplemental Material at http://link.aps.org/supplemental/10.1103/PhysRevB.87.201401 for technical details.
[21] H. W. K. Tom, T. F. Heinz, and Y. R. Shen, Phys. Rev. Lett. **51**, 1983 (1983).
[22] Y. R. Shen, Annu. Rev. Phys. Chem. **40**, 327 (1989).
[23] L. F. Mattheiss, Phys. Rev. B **8**, 3719 (1973).
[24] M. S. Dresselhaus, G. Dresselhaus, and A. Jorio, *Group Theory Applications to the Physics of Condensed Matter* (Springer-Verlag, Berlin, 2008).
[25] L. M. Malard, M. H. D. Guimarães, D. L. Mafra, M. S. C. Mazzoni, and A. Jorio, Phys. Rev. B **79**, 125426 (2009).
[26] Y.-W. Son, M. L. Cohen, and S. G. Louie, Nature (London) **444**, 347 (2006).
[27] G. Giovannetti, P. A. Khomyakov, G. Brocks, P. J. Kelly, and J. van den Brink, Phys. Rev. B **76**, 073103 (2007).
[28] M. Yankowitz, J. Xue, D. Cormode, J. D. Sanchez-Yamagishi, K. Watanabe, T. Taniguchi, P. Jarillo-Herrero, P. Jacquod, and B. J. LeRoy, Nat. Phys. **8**, 382 (2012).
[29] N. Bloembergen and P. S. Pershan, Phys. Rev. **128**, 606 (1962).
[30] N. Kumar, S. Najmaei, Q. Cui, F. Ceballos, P. M. Ajayan, J. Lou, and H. Zhao, Phys. Rev. B **87**, 161403 (2013).
[31] H. Zeng, G.-B. Liu, J. Dai, Y. Yan, B. Zhu, R. He, L. Xie, S. Xu, X. Chen, W. Yao, and X. Cui, Sci. Rep. **3**, 1608 (2013).